Shape-Dependent Multiexciton Emission and Whispering Gallery Modes in Supraparticles of CdSe/Multishell Quantum Dots

Daniël Vanmaekelbergh,*,† Lambert K. van Vugt,† Henriëtte E. Bakker,‡ Freddy T. Rabouw,† Bart de Nijs,‡ Relinde J. A. van Dijk-Moes,† Marijn A. van Huis,‡ Patrick J. Baesjou,‡,§ and Alfons van Blaaderen‡

†Condensed Matter and Interfaces and ‡Soft Condensed Matter, Debye Institute, Utrecht University, Princetonplein 5, 3584 CC Utrecht, The Netherlands and §Philips Research, Photonic Materials & Devices, High Tech Campus, HTC4, 5656AE Eindhoven, The Netherlands

ABSTRACT Semiconductors are indispensable as the active light-emitting element in many optoelectronic devices. However, even the purest bulk semiconductors suffer from considerable nonradiative recombination leading to low photoluminescence efficiencies. Zero-dimensional quantum dots show a much better carrier-to-photon conversion caused by confinement of the excitons but suffer from nonradiative recombination when assembled into a solid, due to exciton energy transfer. Here, we report on the shape-dependent optical properties of self-assembled supraparticles composed of CdSe/multishell nanocrystals. All supraparticles show stable and bright photoluminescence in ambient up to high excitation intensities. When the supraparticles are deposited on a silicon surface their spherical shape is deformed due to drying. In addition to single-exciton emission, we observe bright emission from multiexciton states at high excitation powers. In contrast, supraparticles that retain their perfectly spherical shape show a spectrum with sharp Mie whispering gallery modes, while multiexciton emission is absent.

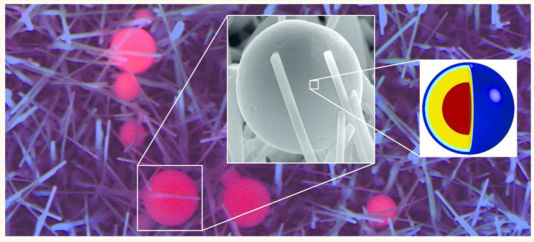

KEYWORDS: quantum dot · nanocrystal · assembly · quantum dot solid · multiexciton emission · whispering gallery mode · Auger recombination

Semiconductors are indispensable as the active light-emitting element in many optoelectronic devices. However, even the purest bulk semiconductors, such as Si or GaAs,[1,2] suffer from considerable nonradiative recombination due to the long carrier or exciton diffusion length, which means that excitons can wander around and find a defect center, eventually. High photoluminescence quantum efficiencies are possible when charge carrier and exciton diffusion are confined, such as in well-prepared quantum wells.[3] Zero-dimensional quantum dots (QDs) can show a very good carrier-to-photon conversion caused by confinement of the excitons in the volume of the QD. However, when nanocrystalline QDs are assembled into a QD solid, exciton energy transfer from QD to QD can occur which again leads to a considerable reduction of the photoluminescence quantum yield.[4−7] The solution of the problem has been to grow a shell, or multiple shells, around the QD. A shell does not only passivate the QD surface but also forms a barrier against exciton wandering by resonant energy transfer.[8,9] Simultaneously, losses due to nonradiative Auger recombination of multiexciton states are reduced in core/shell structures. This many-body process is based on Coulomb interactions that are enhanced in small nanocrystalline QDs compared to a bulk material. Moreover, the abrupt step in the confinement potential at the QD surface, resulting in a large uncertainty in the electron and hole wave vectors, weakens the selection rule for Auger processes and therefore enhances the rate. Only after strong multiexciton emission was observed in self-organized epitaxial InGaAs quantum dots[10] with a shallow and gradual confinement potential, were colloidal analogues developed.[11−15] The same recipe that may prevent exciton energy transfer, *i.e.*, the growth of multiple shells around the nanocrystal, is

* Address correspondence to d.vanmaekelbergh@uu.nl.

Received for review December 22, 2014 and accepted April 6, 2015.

Published online April 06, 2015
10.1021/nn507310f

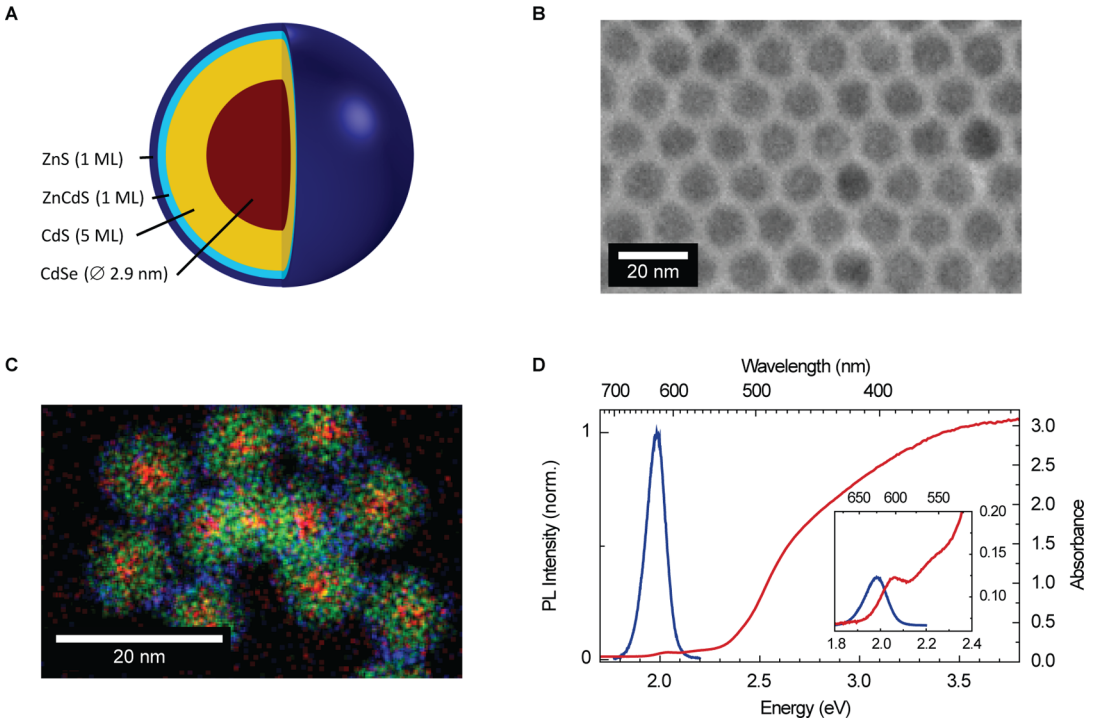

Figure 1. Structure and optical properties of CdSe (core) CdS/CdZnS/ZnS (multishell) quantum dots. (a) Schematic representation of the multishell quantum dot design. (b) Bright-field TEM image of a self-assembled 2D colloidal crystal lattice consisting of multishell quantum dots. (c) High-resolution STEM-EDS quantified chemical map of individual multishell nanocrystals showing a Se containing core (red) surrounded by a S-containing shell (green) and an outmost Zn-containing shell (blue). Separate elemental maps are shown in the Supporting Information (Figure S4). (d) PL emission (left axis) and linear absorption (right axis) spectra of the multishell quantum dots in toluene. The absorption is dominated by interband absorption in the CdS shell at energies above ~2.4 eV. A magnification of the region below the CdS bandgap (inset) shows the optical transitions in the CdSe core.

used to make the confinement potential less abrupt and in this way reduce the rate of Auger recombination. Recently, suppressed Auger recombination and related to that increased multiexciton emission have been reported for several types of specially engineered multishell nanocrystalline QDs.[13,16−21]

Here we report on the optical properties of a special type of QD solids that are assembled from CdSe (core) CdS/CdZnS/ZnS (multishell) QDs. These solids have a scalable spherical shape in the colloidal domain. Notwithstanding the (nearly) spherical shape, the QDs in the supraparticles are ordered. Provided that such supraparticles are still emitting, they would enable new designs for biological labels, LEDs and lighting, lasing, and optical switching.[14,22−24] In the literature, supraparticles are also referred to as superparticles and have previously been made using roughly two pathways: one involves attractions such as hydrophobic forces between the particles[25−27] and the other uses drying emulsion droplets.[28,29] With an emulsion-based method in which self-assembly of nanoparticles takes place in droplets[30] we have prepared supraparticles of CdSe core/multishell QDs. The supraparticles have a perfectly spherical shape dictated by surface tension and diameters from 0.1 to several μm if the particles are deposited without drying effects, *e.g.*, by sublimation of the suspending solvent.[30] The shape is also retained when these supraparticles are deposited on a field of ZnO nanowires. However, when these supraparticles are deposited on a silica surface, drying forces distort the spherical shape.

We investigate the light emission from these supraparticles and how it depends on the supraparticle shape. In all cases, the supraparticles are photochemically stable in air up to high excitation intensities and show a high photoluminescence quantum yield. The supraparticles deformed by drying effects show strong and bright exciton emission, without a reduction of the yield by exciton energy transfer. In addition, they feature strong blue-shifted multiexciton emission at higher excitation intensities. Sufficiently large *spherical* supraparticles (>1.5 μm) show a constant emission spectrum over five orders of excitation intensity with sharp peaks related to optical whispering gallery modes, while multiexciton emission is absent. It is clear that the optical properties of QD supraparticles depend both on the properties of the individual core−shell QDs and on collective effects of the supraparticle shape.

RESULTS AND DISCUSSION

Assembly of Core/Multishell Quantum Dots into Supraparticles. The synthesis of the CdSe (core) CdS/CdZnS/ZnS (multishell) QDs and the formation of spherical supraparticles of these QDs is detailed in the Supporting

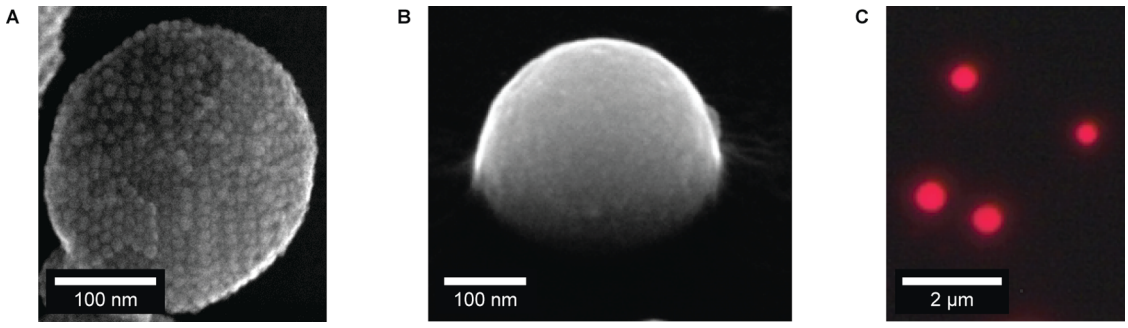

Figure 2. Structure of self-assembled supraparticles of CdSe (core) CdS/CdZnS/ZnS (multishell) quantum dots. (a) SEM image of an individual supraparticle, clearly showing the constituent nanocrystals. (b) 52° side view image of an individual supraparticle on a SiO_2 substrate, showing that the shape is distorted from spherical due to drying forces. (c) Microscope image of the supraparticles on a SiO_2 substrate under UV excitation at 349 nm.

Information. Parts a−c of Figure 1 show the structures of the core−shell QDs, which are sufficiently monodisperse to self-assemble into ordered colloidal crystals (Figure 1b). Photoluminescence (PL) and linear absorption (LA) spectra at low excitation intensity of the QDs in cyclohexane (Figure 1d) show that the emission is centered at 1.98 eV (630 nm) with the lowest core absorption transition at 2.03 eV (611 nm) (inset), both markedly lower (∼255 meV) than for the bare CdSe cores (see the Supporting Information, Figure S2a), pointing to a loss of confinement of the exciton due to the multiple-shell geometry. Above the energy of the bulk band gap of CdS (2.4 eV), the LA spectrum of the QDs is dominated by the featureless CdS shell absorption, with a large absorption cross-section of 5×10^{-15} cm^2 at 3.55 eV. We measured the PL quantum yield (QY) with an integrating sphere to be in the 50−55% range.

Self-assembly in slowly drying oil droplets resulted in spherical supraparticles with a diameter between 100 nm and several μm (Figure 2a). When these supraparticles are deposited on a silica substrate their shape is deformed by drying (Figure 2b), but they still emit bright red light (Figure 2c). Remarkably, when the QDs are self-assembled into supraparticles and dispersed in water, the PL quantum yield remains as high as 50−55%, similar to that of the individual QDs in suspension (Supporting Information, Figure S1). This is in contrast with the results obtained with solids of bare CdSe nanocrystals in which the luminescence gets nearly completely quenched.[4,31] It means that when assembled in a (supraparticle) solid the emitting cores of our core/shell QDs are situated sufficiently far from each other that quantum mechanical wave function overlap and Förster energy transfer between the QDs are absent.

Multiexciton Emission. Under high-intensity pulsed laser excitation (5 ns pulses at 349 nm), the PL emission spectrum of suspensions of the QDs or individual supraparticles on a silica substrate extends to higher energies by about 240 meV (Figure 3a,b). Aside from the original emission centered around 1.98 eV, now distinct peaks at 2.12 and 2.34 eV also appear with a remarkably high intensity. By again lowering the laser excitation intensity these peaks disappear and the spectrum reverts back to the one presented in Figure 1d, showing that the extension of the emission spectrum to higher energy is a reversible electronic effect and is not due to a structural modification. The reversible change in the emission spectrum is observed for individual QDs in suspension as well as for supraparticles on a silica substrate. The supraparticles are photochemically stable and a gradual deterioration of the total intensity is only observed at very high fluences of $>10^{-2}$ J/cm^{-2}.

As we discuss in more detail below, the extension of the emission spectrum to higher energy is due to emission from several multiexciton states, enabled by the suppression of Auger rates in core/shell QDs. While suppression of Auger rates in core/shell QDs has been investigated and confirmed in several recent (time-resolved) studies,[11−15,24,32−34] QD solids, such as the supraparticles presented here, with strong multiexciton emission have not been reported previously.

Parts c and d of Figure 3 demonstrate (for individual QDs in Figure 3c and for a supraparticle in Figure 3d) that the intensities of the high-energy emission peaks increase nearly linearly in intensity with the pump power, with a slope of ∼1.2 on a log−log scale. To understand such low powers in the power dependence of multiexciton emission, it is important to realize that our excitation pulse width is 5 ns. Consequently, the system can reach a steady state during a laser pulse. We confirm this in Figure S3 (Supporting Information) with a four-level rate equation model including the ground state, the single exciton, the biexciton, and the triexciton. At steady state the population of the triexciton is

$$N_{X_3} = \frac{P^3}{k_1k_2k_3 + k_2k_3P + k_3P^2 + P^3} \quad (1)$$

where P is the pump rate (absorption events/unit of time) and $k_{1,2,3}$ are the decay rates from exciton, biexciton, and triexciton. We see that the power

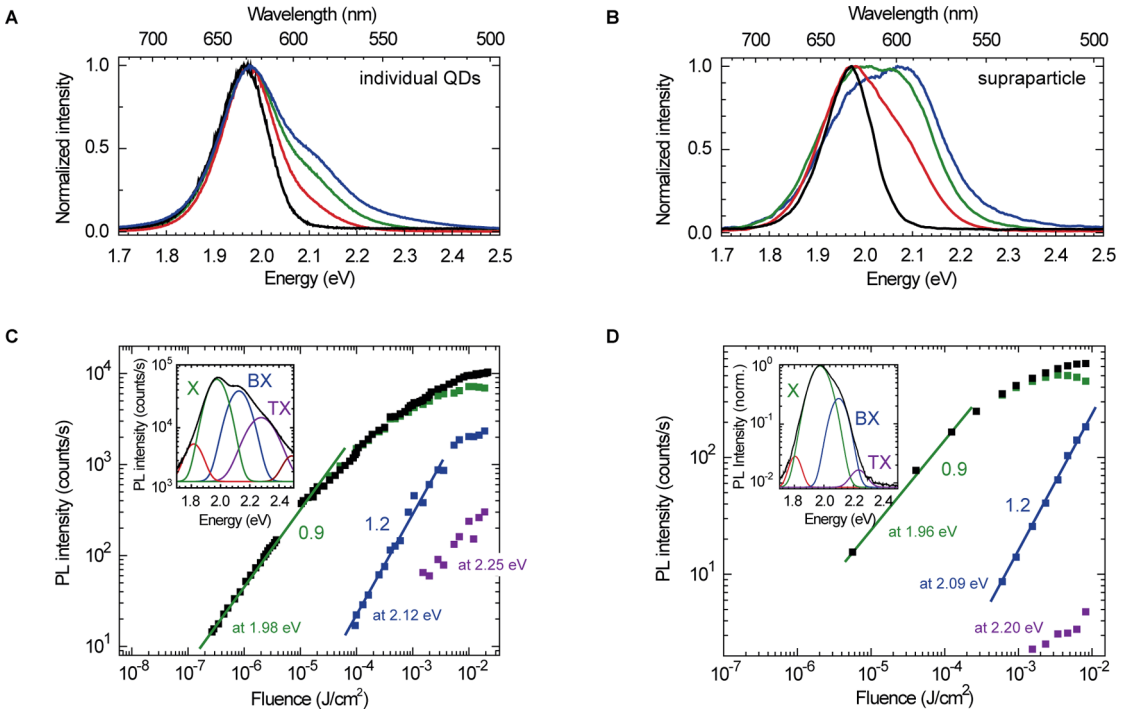

Figure 3. Excitation intensity dependent emission spectra of CdSe (core) CdS/CdZnS/ZnS (multishell) quantum dots in suspension and self-assembled supraparticles. (a) PL emission spectra of a solution of multishell quantum dots at excitation fluences of 1.1×10^{-6} (black), 1.0×10^{-4} (red), 1.0×10^{-3} (green), and 1.9×10^{-3} J/cm^2 (blue), demonstrating the emergence of high-energy peaks at 2.12 and 2.34 eV at intense excitation in addition to the peak at 1.98 eV already present at low excitation intensity. (b) Same as in a, but for an individual supraparticle of 1.3 μm diameter and at excitation fluences of 1.2×10^{-4} (black), 3.4×10^{-3} (red), 6.2×10^{-3} (green) and 8.2×10^{-3} J/cm^2 (blue). (c, d) The integrated emission intensity of each of the optical transitions as a function of the excitation intensity, for (c) individual QDs in dispersion and (d) a supraparticle. The insets show, on a logarithmic scale, how a spectrum is decomposed. The peaks are ascribed (see text) to emission from the single exciton (X; green), the biexciton (BX; blue), and the triexciton or charged biexciton (TX; purple). The additional weak red bands at the low and high energy sides were needed to properly account for small deviations of the emission band shapes from perfectly Gaussian. For all panels, the excitation is at 349 nm, with a repetition rate of 5 kHz and a pulse duration of 10 ns.

dependence of the triexciton emission can be near linear if the third term in the denominator is much larger than the second and the first (*i.e.*, $P \gg k_2$). Since the blueshifted emission can be assigned to triexcitons (see below), the experimental slope of 1.2 (Figures 3c,d) is related to relatively slow biexciton decay (k_2) confirming the suppression of Auger processes in our multishell QDs. The fact that also in a scalable nano- to microsized colloid particle composed of QDs Auger recombination can be suppressed efficiently, is encouraging for high-intensity applications in lighting and biological research.

Characterization of the Multiexciton States. In order to elucidate the microscopic nature of the emission bands, we performed detailed excitation−emission spectroscopy for variable excitation intensity. Parts a−d of Figures 4 present the PL excitation−emission maps for the suspension of individual QDs (a, b) and a supraparticle (c, d). The dashed blue line in Figure 4f presents the excitation spectrum of the QD solution at low intensity lamp excitation. In the energy range before the onset of CdS shell absorption (2.4 eV), a clear structure is seen originating from discrete optical transitions in the CdSe core. At higher excitation intensities, the excitation map (Figure 4b) and spectrum (dashed red line in Figure 4f) show the same resonances. In addition, the excitation−emission maps (Figure 4c,d) and excitation spectra (solid lines in Figure 4f) of a supraparticle show qualitatively the same behavior as the QD solution. This demonstrates that the intrinsic exciton states are preserved when the QDs are assembled into supraparticles. We see in Figure 4f that the apparent strength of the CdS interband transitions (above 2.4 eV) is lower at high excitation power (red) than at low power (blue). This can be understood because at high power we saturate the single-exciton emission, as apparent from the decreasing slopes in Figure 3c,d. Consequently, spectral variations in absorption strength appear weaker in the high-power excitation spectrum.

The additional emission bands at high pump power blueshifted from the exciton emission must originate from multicarrier states. These can be simple multiexciton states of several electron−hole pairs per QD), but they can also be charged states. Multiexciton states can be generated at high pump powers by rapid successive absorption of multiple photons. Indeed, the CdS shell strongly absorbs excitation light in the UV and funnels excitons to the core. At the same time, strong excitations conditions are known to be able to

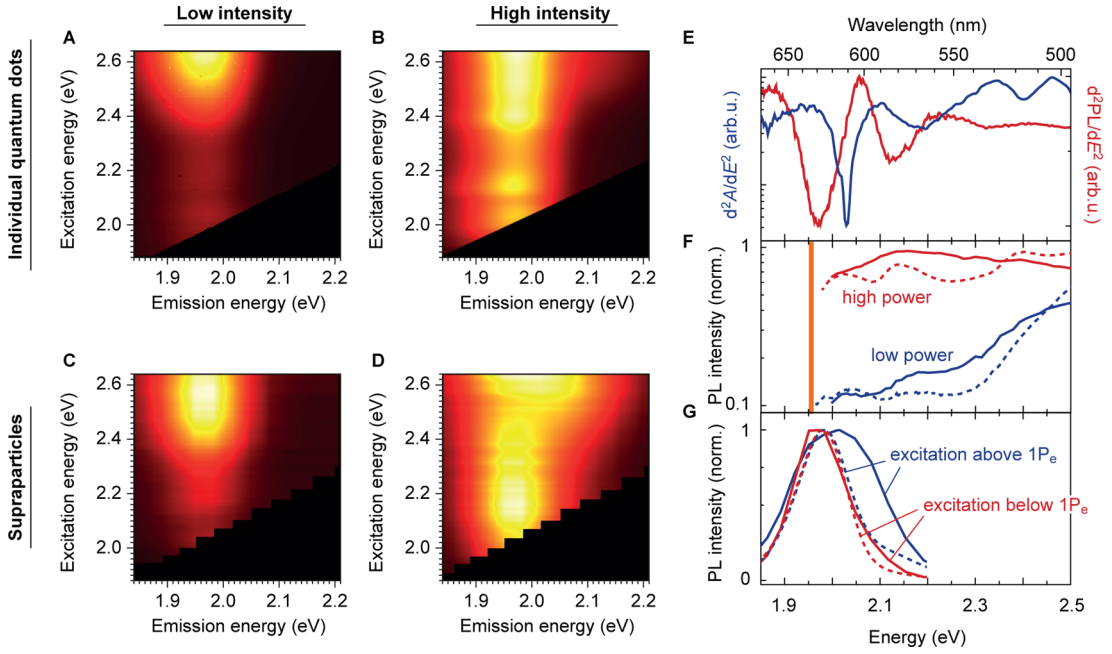

Figure 4. PL emission and excitation spectra as a function of excitation intensity. (a, b) Excitation−emission maps of a quantum-dot solution at (a) low and (b) high ($\sim 10^{-3}$ J/cm^2) excitation intensity. (c, d) Same but for an individual supraparticle on a SiO_2 substrate. (e) Second derivative of the absorption spectrum (blue line, left axis) and the high-excitation intensity PL spectrum (red line, right axis) of a quantum dot solution. (f) Excitation spectra of the quantum dot solution (dashed lines) and the supraparticle (solid lines) for emission at 1.96 eV at low (blue) and high (red) excitation intensity, extracted from panels a−d. (g) Cross-cuts through panels b,d: emission spectra of the quantum dot solution (dashed lines) and the supraparticle (solid lines) at high excitation intensity. Excitation is at 2.3 eV (red; below the $1P_{3/2}1P_e$ absorption) or at 2.6 eV (blue; above the $1P_{3/2}1P_e$ absorption). Data were corrected for spectral variations in the output power of the excitation sources.

result in charge ejection (more precisely, Auger ejection from a multiexciton state[35,36]) leaving the QD with a net charge. This is one of the mechanisms believed to be responsible for QD blinking.

Since the pronounced shoulders in the emission spectrum (Figure 3a,b) are blueshifted by >150 meV with respect to the exciton emission we conclude that they are not simply due to biexcitons or charged single excitons (*i.e.*, trions) because the binding energies of these are usually no more than a few 10 meV.[37] Instead, they must be higher multicarrier states. In conventional QDs, emission from such states would be strongly quenched by Auger processes. We observe them in emission by virtue of suppressed Auger recombination in our core/multishell QDs. Indeed, emission from triexcitons and charged biexcitons[15,38−42] has been observed before in core/shell QDs.

To identify to which possible multicarrier states the blue-shifted emission bands can be ascribed, we first assign the transitions in the absorption spectrum of our core/shell QDs. The blue line in Figure 4e shows the second derivative of the absorption spectrum, with three pronounced dips at 2.03, 2.18, and 2.39 eV. Following Norris and Bawendi,[42] we ascribe these to the $1S_{3/2}1S_e$, $2S_{3/2}1S_e$, and $1P_{3/2}1P_e$ exciton transitions. For additional confirmation that the peak positions are as expected, we discuss in Figure S2 (Supporting Information) the red shift of absorption peaks of CdSe QDs upon growth of a CdS shell.[43] From the absorption spectrum we can estimate the energies of the excited single-particle states, using the known values in core-only CdSe QDs.[44] Since in a CdSe/CdS core/shell structure the hole is tightly confined to the core, we estimate that the $1S_{3/2}-1P_{3/2}$ and $1S_{3/2}-2S_{3/2}$ splittings in the valence band in our core/multishell QDs are the same as in core-only QDs: 35 and 150 meV, respectively.[45] The electron $1S_e-1P_e$ splitting must then be 325 meV, lower than the 500 meV in core-only QD due to electron delocalization in the shell. Based on these values extracted for the single-particle energy levels, we can assign the multicarrier emission bands observed in the strong excitation limit.

The red line in Figure 4e shows the second derivative of the PL emission spectrum of individual QDs in dispersion at high excitation powers. The dominant transition at 1.97 eV is ascribed to the $1S_{3/2}1S_e$ exciton, Stokes shifted with respect to the absorption by 60 meV. We see two other transitions at 2.12 and 2.31 eV. To assign these it is important to realize that multicarrier states can be thought of as a combination of single-carrier states only as a first-order approximation. The energies and selection rules for transitions become affected by carrier interactions as the number of free carriers increases. It is even possible that carrier interactions affect the order in which single-carrier levels are occupied.[46]

Emission peaks blue-shifted by more than 100 meV from the $1S_{3/2}1S_e$ single exciton emission have previously

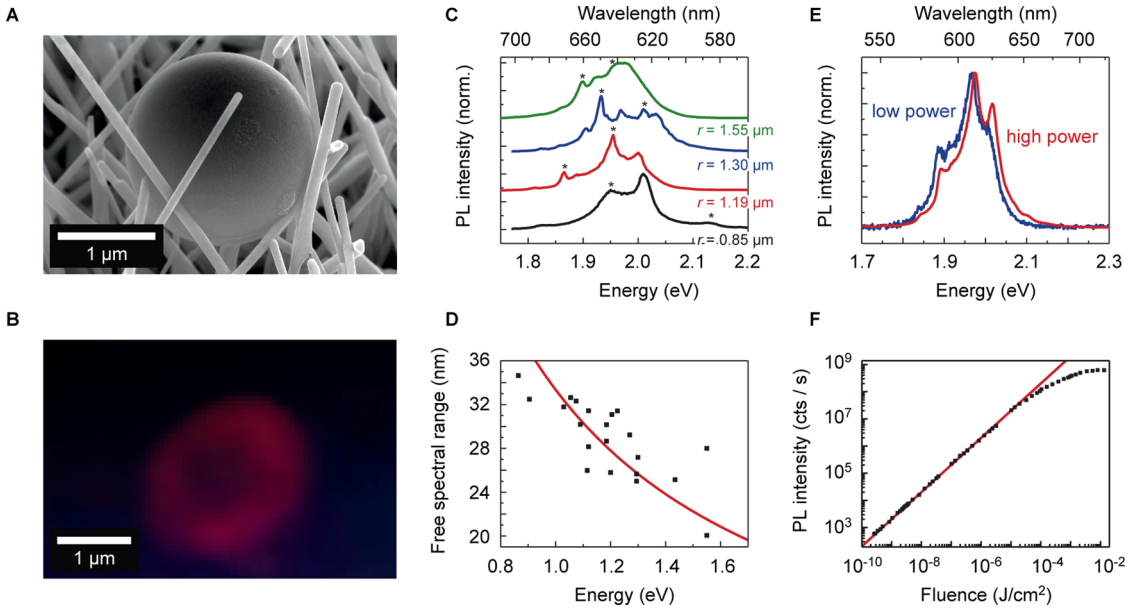

Figure 5. Mie whispering gallery modes in supraballs. (a) SEM image of a supraball lying on a field of ZnO nanowires. (b) Microscope image of a supraball on ZnO nanowires under quasi-continuous excitation (5 ns pulses) in the UV at 349 nm, showing more intense emission at the circumference owing to whispering gallery modes. (c) PL emission spectra of four supraballs of different radius, showing spectral features related to the whispering gallery mode structure. (d) Free spectral range $\Delta\lambda$ of the modes *versus* the supraball radius r. The red line is a fit to $\Delta\lambda = \lambda^2/2\pi r n_g$ with a group refractive index $n_g = 1.89$. The asterisks in c indicate modes belonging to mode families with incremental quantum number. (e) Two emission spectra of an individual supraparticle, one at low excitation fluence (1.06×10^{-9} J/cm^2, blue), and one at orders of magnitude higher excitation intensity (9.7×10^{-4} J/cm^2, red). (f) Integrated PL emission intensity as a function of the pump fluence. There is a linear dependence over 6 orders of magnitude in fluence.

been ascribed to states with a $1P_e$ electron: triexcitons[39−42] or negative charged biexcitons.[15,38] In this work, we observe two clear blueshifted bands (see insets of Figure 3c,d), which we assign to states with more than four charge carriers. These could be either triexcitons or charged biexcitons, which would emit at roughly the same wavelength because the same single-carrier states are occupied. Previous assignments of the single-carrier states involved in the blueshifted transitions have been ambiguous. Here, we hypothesize that the transition at 2.12 eV (blueshifted by 150 meV) is a $1S_{3/2}1S_e$ transition, of which the energy is blueshifted by virtue of a repulsive multicarrier interactions. The transition at 2.31 eV (blueshifted by 340 meV) must involve a $1P_e$ electron. It can either be a $1S_{3/2}1P_e$ transition (that became allowed by multicarrier interactions[38]) or a $1P_{3/2}1P_e$ transition (where the $1P_{3/2}$ hole state is occupied either thermally[39] or by multicarrier interactions[46]). The assignment of the blueshifted peak to states containing a $1P_e$ electron is confirmed in the emission spectra of Figure 4g: the blueshifted emission only appears if we excite above (blue) the $1P_{3/2}1P_e$ absorption resonance, not below (red).

Whispering Gallery Modes in Spherical Supraparticles. The exciton and multiexciton emission was observed for supraparticles with a nonspherical shape deposited on a silica substrate. However, when the supraparticles particles were deposited on a field of upstanding ZnO nanowires their spherical shape was retained, most likely as during drying the water was drained through the layer of rods (see Figure 5a) circumventing deformation of the spherical supraparticles. The emission spectra of individual supraparticles show sharp peaks in the energy region around 2 eV at all pump powers, while their microscope images show the signs of whispering gallery modes (Figure 5b,c). Similar whispering gallery modes were observed previously with much larger silica microspheres on which quantum dots were adsorbed.[47,48] From the peak widths we derive a quality factor of the whispering gallery modes of Q = fwhm/$\lambda \sim 100$. Figure 5d presents the free spectral range of the modes (for instance, those indicated with stars in Figure 5c) plotted as a function of the radius of the supraparticles. The line gives the free spectral range calculated for whispering gallery modes in spheres of varying diameter using $\Delta\lambda = \lambda^2/(2\pi r_{ball} n_g)$, with a group refractive index n_g of 1.89 and the emission wavelength λ taken as 630 nm. Remarkably, the shape of the emission spectrum remains perfectly constant over 5 orders of excitation intensity (Figure 5e). This also means that, unlike for the deformed supraparticles, multiexciton emission does not occur at higher excitation intensities. This difference might be related to the higher density of optical states (DOS; averaged over the emission spectrum of the QDs) due to Mie resonances in a supraball. A higher DOS leads to faster decay rates ($k_{1,2,3}$ in eq 1) for all single and multiexciton states. Consequently, the fluence required to reach a

considerable multiexciton population can become much higher. The unchanged shape of the emission spectrum with sharp peaks related to whispering gallery modes also shows that there is no gain for these modes. Indeed, Figure 5f shows that the intensity of the entire spectrum increases linearly with the excitation intensity. The reason for the absence of gain and lasing is not yet clear. It might be related to the relatively small diameter of our supraballs (maximum 3 μm) or optical coupling of the supraballs with the supporting ZnO nanowires.[49,50]

CONCLUSION

In summary, we have demonstrated that quantum dot supraparticles with a nonspherical shape show stable and bright broadband emission from exciton and multiexciton states with a similar quantum yield as individual QDs in dispersion. The PL efficiency of these scalable solid-state systems of about 55% surpasses that of the purest single crystalline bulk semiconductors. Spherical supraparticles emit from whispering gallery modes fed by the lowest exciton states. We have, hence, developed a class of bright QD supraparticles with a scalable size, the optical properties of which can be tuned by their shape. Individual supraparticles, which can be made with diameters from 100 nm to micrometers, can have high potential in applications varying from biolabeling to integration with waveguides in silicon nitride optoelectronics. Moreover, although lasing from these supraparticles was not observed yet, we believe that finding the conditions such that the Mie modes that we found also show gain and finally lead to supraparticle lasing is a question of time. Finally, we remark that spherical supraparticles are colloids, for which microfluidic methods are available to reduce the size dispersion. This means that it should be possible to further assemble the supraparticles in a third step in hierarchy to form photonic crystals for optical wavelengths. Hence, our results also open new versatile three-step routes for scalable fabrication of photonic structures.

METHODS

Quantum Dot and Supraparticle Synthesis. All QD syntheses were performed in an oxygen-free atmosphere with predried chemicals and stored in a glovebox. CdSe nanocrystal cores were synthesized using a modified Peng method,[51] while for the shell growth the Silar method was used.[52] A detailed description of the syntheses can be found in the Supporting Information. For a typical supraball synthesis,[30] 1 mL of cyclohexane containing 7 mg of nanocrystals was mixed with 10 mL of deionized water containing 400 mg of dextran (mol wt 1.500−2.800 kDa) and 60 mg of sodium dodecyl sulfate. The mixture was then sheared using a Couette rotor−stator device (gap spacing 0.3 mm). The resulting emulsion was heated to 68 °C and kept at this temperature for 4 h, evaporating the cyclohexane, and the suspension was then allowed to cool to room temperature and washed twice by sedimenting and redispersing in deionized water. The size of the supraballs can be changed by varying the shear rate (1000 rpm-7000 rpm), gap spacing (0.1 mm-0.4 mm), and the concentration of nanocrystals in the initial cyclohexane solution.

Optical Measurements. Optical measurements were performed on samples consisting of dilute nanocrystal chloroform solutions (2×10^{-6} mol/L) in either a quartz cuvette or a capillary. We also investigated individual supraparticles lying on a 600 nm SiO_2 covered Si substrate and immersed in Leica immersion oil type F. Five different optical setups were used: (1) an Edinburgh instruments F900 double spectrometer (Figures 1d and 4a); (2) PerkinElmer lambda 950 spectrophotometer (inset Figure 1d); (3a) a home-built luminescence microscope fitted with pulsed laser excitation (Spectra Physics Explorer, 349 nm, 5 ns pulse duration, 5 kHz repetition rate) attenuated with neutral density filters and focused to an 50 μm fwhm spot coupled to a liquid nitrogen cooled spectrometer/CCD (Princeton instruments) (Figures 3 and 5); (3b) the same-home-built microscope but fitted with a pulsed tunable laser (Opotek Opolette 355, 10 ns, 10 Hz repetition rate) (Figure 4b); (4) a Leica TCS SP8 confocal microscope fitted with an pulsed super continuum source (NKT Photonics, 5 ps pulse duration, 78 MHz repetition rate), focusing objective (63 × /1.32 NA oil-immersion confocal objective (LEICA), and PMT detection (Figures 4c,d); and (5) absolute QY measurements (Supporting Information, Figure S1) were performed on chloroform nanocrystal solutions and water solutions of supraballs using 445 nm diode laser excitation, a Labsphere 6 in. integrating sphere and a fiber coupled spectrometer (USB 4000, Ocean Optics). The combination of sphere, fiber, and spectrometer was calibrated with a light source of known emission characteristics.

Electron Microscopy. The bright-field TEM images were obtained with an FEI Tecnai F-20. SEM images were obtained with an FEI Nova 600 nanolab. HAADF−STEM (high angle annular dark field scanning transmission electron microscopy) images and STEM−EDS (scanning transmission electron microscopy energy dispersive X-ray spectrometry) maps of individual nanocrystals were obtained with a JEOL ARM200F equipped with a 100 mm^2 SDD detector for EDS, operating at 200 kV. The semiconvergence angle was 25 mrad, and the 256 × 256 pixel maps in Figure 1c and Figure S5 (Supporting Information) were recorded with a dwell time of 0.1 ms (87 frames).

Conflict of Interest: The authors declare no competing financial interest.

Acknowledgment. This work is supported by NanoNextNL, a micro- and nanotechnology consortium of the Government of The Netherlands and 130 partners. This work is part of the research programme of FOM, which is part of The Netherlands Organization for Scientific Research (NWO). Part of the research leading to these results has received funding from the European Research Council under the European Union Seventh Framework Programme (FP/2007-2013)/ERC Grant Agreement No. 291667. We gratefully thank JEOL, Ltd., E. Okunishi, C. T. W. M. Schneijdenberg, and J. D. Meeldijk for the high-resolution STEM-EDS measurements. R.J.A.v.D.-M. synthesized the multishelled quantum dots and performed low-resolution TEM. B.d.N. performed the self-assembly into supraballs. M.A.v.H. performed the interpretation of the STEM-EDS measurements, and P.J.B. performed QY measurements. H.E.B. measured the single supraparticle excitation maps. L.K.v.V. performed all other spectroscopy measurements, SEM measurements, and integrated the data. D.V., L.K.v.V., H.E.B., F.T.R., and A.v.B. interpreted the data. D.V., L.K.v.V, F.T.R. and A.v.B. wrote the manuscript with the help of all other coauthors.

Supporting Information Available: Synthesis of core/multishell quantum dots, determination of quantum yield of multishell quantum dots and supraparticles, evolution of the optical resonances from core-only to core multishell nanocrystals,

power dependence of multiexciton emission, and chemical mapping of the multishell quantum dots using STEM-EDS. This material is available free of charge *via* the Internet at http://pubs.acs.org.

REFERENCES AND NOTES

1. Green, M. A.; Zhao, J. H.; Wang, A. H.; Reece, P. J.; Gal, M. Efficient Silicon Light-Emitting Diodes. *Nature* **2001**, *412*, 805–808.
2. Green, M. A. Radiative Efficiency of State-of-the-Art Photovoltaic Cells. *Prog. Photovolt. Res. Appl.* **2012**, *20*, 472–476.
3. Schnitzer, S. A.; Yablonovitch, E.; Caneau, C.; Gmitter, T. J. Ultrahigh Spontaneous Emission Quantum Efficiency, 99.7% Internally and 72% Externally, from AlGaAs/GaAs/AlGaAs Double Heterostructures. *Appl. Phys. Lett.* **1993**, *62*, 131–133.
4. Crooker, S. A.; Hollingsworth, J. A.; Tretiak, S.; Klimov, V. I. Spectrally Resolved Dynamics of Energy Transfer in Quantum-Dot Assemblies: Towards Engineered Energy Flows in Artificial Materials. *Phys. Rev. Lett.* **2012**, *89*, 186802.
5. Achermann, M.; Petruska, M. A.; Crooker, S. A.; Klimov, V. I. Picosecond Energy Transfer in Quantum Dot Langmuir-Blodgett Nanoassemblies. *J. Phys. Chem. B* **2003**, *107*, 13782–13787.
6. Song, H.; Lee, S. Red Light Emitting Solid State Hybrid Quantum Dot-Near-UV GaN LED Devices. *Nanotechnology* **2007**, *18*, 255202.
7. Kagan, C. R.; Murray, C. B.; Nirmal, M.; Bawendi, M. G. Electronic Energy Transfer in CdSe Quantum Dot Solids. *Phys. Rev. Lett.* **1996**, *76*, 3043–3043.
8. Zhao, J.; Chen, O.; Strasfeld, D. B.; Bawendi, M. G. Biexciton Quantum Yield Heterogeneities in Single CdSe (CdS) Core (Shell) Nanocrystals and Its Correlation to Exciton Blinking. *Nano Lett.* **2012**, *12*, 4477–4483.
9. Hines, M. A.; Guyot-Sionnest, P. Synthesis and Characterization of Strongly Luminescing ZnS-Capped CdSe Nanocrystals. *J. Phys. Chem.* **1996**, *100*, 468–471.
10. Dekel, E.; Gershoni, D.; Ehrenfreund, E.; Spektor, D.; Garcia, J. M.; Petroff, P. M. Multiexciton Spectroscopy of a Single Self-Assembled Quantum Dot. *Phys. Rev. Lett.* **1998**, *80*, 4991–4994.
11. Javaux, C.; Mahler, B.; Dubertret, B.; Shabaev, A.; Rodina, A. V.; Efros, Al. L.; Yakovlev, D. R.; Liu, F.; Bayer, M.; Camps, G.; et al. Thermal Activation of Non-Radiative Auger Recombination in Charged Colloidal Nanocrystals. *Nat. Nanotechnol.* **2013**, *8*, 206–212.
12. Cragg, G. E.; Efros, A. L. Suppression of Auger Processes in Confined Structures. *Nano Lett.* **2010**, *10*, 313–317.
13. Park, Y.-S.; Malko, A. V.; Vela, J.; Chen, Y.; Ghosh, Y.; García-Santamaría, F.; Hollingsworth, J. A.; Klimov, V. I.; Htoon, H. Near-Unity Quantum Yields of Biexciton Emission from CdSe/CdS Nanocrystals Measured Using Single-Particle Spectroscopy. *Phys. Rev. Lett.* **2011**, *106*, 187401.
14. Garcia-Santamaria, F.; Brovelli, S.; Viswanatha, R.; Hollingsworth, J. A.; Htoon, H.; Crooker, S. A.; Klimov, V. I. Breakdown of Volume Scaling in Auger Recombination in CdSe/CdS Heteronanocrystals: The Role of the Core-Shell Interface. *Nano Lett.* **2011**, *11*, 687–693.
15. Htoon, H.; Malko, A. V.; Bussian, D.; Vela, J.; Chen, Y.; Hollingsworth, J. A.; Klimov, V. I. Highly Emissive Multiexcitons in Steady-State Photoluminescence of Individual "Giant" CdSe/CdS Core/Shell Nanocrystals. *Nano Lett.* **2010**, *10*, 2401–2407.
16. Chen, O.; Wei, H.; Maurice, A.; Bawendi, M.; Reiss, P. Pure Colors from Core-Shell Quantum Dots. *MRS Bull.* **2013**, *38*, 696–702.
17. Osovsky, R.; Cheskis, D.; Kloper, V.; Sashchluk, A.; Kroner, M.; Lifshitz, E. Continuous-Wave Pumping of Multiexciton Bands in the Photoluminescence Spectrum of a Single CdTe-CdSe Core-Shell Colloidal Quantum Dot. *Phys. Rev. Lett.* **2009**, *102*, 197401.
18. Park, Y.-S.; Bae, W. K.; Padilha, L. A.; Pietryga, J. M.; Klimov, V. I. Effect of the Core/Shell Interface on Auger Recombination Evaluated by Single-Quantum-Dot Spectroscopy. *Nano Lett.* **2014**, *14*, 396–402.
19. Minotto, A.; Todescato, F.; Signorini, R.; Jasieniak, J. J.; Bozio, R. Influence of Core-Shell Interfaces on Exciton and Multi-Exciton Dynamics of CdSe-$Cd_xZn_{1-x}S$ Quantum Dots. *Proc. SPIE* **2014**, *9161*.
20. Marceddu, M.; Saba, M.; Quochi, F.; Lai, A.; Huang, J.; Talapin, D. V.; Mura, A.; Bongiovanni, G. Charged Excitons, Auger Recombination and Optical Gain in CdSe/CdS Nanocrystals. *Nanotechnology* **2012**, *23*, 015201.
21. Lutich, A. A.; Mauser, C.; Da Como, E.; Huang, J.; Vaneski, A.; Talapin, D. V.; Rogach, A. L.; Feldmann, J. Multiexcitonic Dual Emission in CdSe/CdS Tetrapods and Nanorods. *Nano Lett.* **2010**, *10*, 4646–4650.
22. Mashford, B. S.; Stevenson, M.; Popovic, Z.; Hamilton, C.; Zhou, Z.; Breen, C.; Steckel, J.; Bulovic, V.; Bawendi, M.; Coe-Sullivan, S.; et al. High-Efficiency Quantum-Dot Light-Emitting Devices with Enhanced Charge Injection. *Nat. Photonics* **2013**, *7*, 407–412.
23. Mashford, B. S.; Nguyen, T.-L.; Wilson, G. J.; Mulvaney, P. All-Inorganic Quantum-Dot Light-Emitting Devices Formed *via* Low-Cost, Wet-Chemical Processing. *J. Mater. Chem.* **2010**, *20*, 167–172.
24. García-Santamaria, F.; Chen, Y.; Vela, J.; Schaller, R. D.; Hollingsworth, J. A.; Klimov, V. I. Suppressed Auger Recombination in "Giant" Nanocrystals Boosts Optical Gain Performance. *Nano Lett.* **2009**, *9*, 3482–3488.
25. Sánchez-Iglesius, A.; Grzelczak, M.; Altantzis, T.; Goris, B.; Pérez-Juste, P.; Bals, S.; Van Tendeloo, G.; Donaldson, S. H., Jr.; Chmelka, B. F.; Israelachvili, J. N.; et al. Hydrophobic Interactions Modulate Self-Assembly of Nanoparticles. *ACS Nano* **2012**, *6*, 11059–11065.
26. Xia, Y.; Tang, Z. Monodisperse Inorganic Supraparticles: Formation Mechanism, Properties and Applications. *Chem. Commun.* **2012**, *48*, 6320–6336.
27. Wang, T.; LaMontagne, D.; Lynch, J.; Zhuang, J.; Cao, Y. C. Colloidal Superparticles from Nanoparticle Assembly. *Chem. Soc. Rev.* **2013**, *42*, 2804–2823.
28. Qiu, P.; Jensen, C.; Charity, N.; Towner, R.; Mao, C. Oil Phase Evaporation-Induced Self-Assembly of Hydrophobic Nanoparticles into Spherical Clusters with Controlled Surface Chemistry in an Oil-in-Water Dispersion and Comparison of Behaviors of Individual and Clustered Iron Oxide Nanoparticles. *J. Am. Chem. Soc.* **2010**, *132*, 17724–17732.
29. Lee, S. Y.; Gradon, L.; Janeczko, S.; Iskandar, F.; Okuyama, K. Formation of Highly Ordered Nanostructures by Drying Micrometer Colloidal Droplets. *ACS Nano* **2010**, *4*, 4717–4724.
30. De Nijs, B.; Dussi, S.; Smallenburg, F.; Meeldijk, J. D.; Groenendijk, D. J.; Filion, L.; Imhof, A.; Van Blaaderen, A.; Dijkstra, M. Entropy-Driven Formation of Large Icosahedral Colloidal Clusters by Spherical Confinement. *Nat. Mater.* **2015**, *14*, 56–60.
31. Kohn, E.; Lambright, S.; Khon, D.; Smith, B.; O'Connor, T.; Moroz, P.; Imboden, M.; Diederich, G.; Perez-Bolivar, C.; Anzenbacher, P.; et al. Inorganic Solids of CdSe Nanocrystals Exhibiting High Emission Quantum Yield. *Adv. Funct. Mater.* **2012**, *22*, 3714–3722.
32. Dennis, A. M.; Mangum, B. D.; Piryatinski, A.; Park, Y.-S.; Hannah, D. C.; Casson, J. L.; Williams, D. J.; Schaller, R. D.; Htoon, H.; Hollingsworth, J. A. Suppressed Blinking and Auger Recombination in Near-Infrared Type-II InP/CdS Nanocrystal Quantum Dots. *Nano Lett.* **2012**, *12*, 5545–5551.
33. Spinicelli, P.; Buil, S.; Quélin, X.; Mahler, B.; Dubertret, B.; Hermier, J.-P. Bright and Grey States in CdSe-CdS Nanocrystals Exhibiting Strongly Reduced Blinking. *Phys. Rev. Lett.* **2009**, *102*, 136801.
34. Bae, W. K.; Padilha, L. A.; Park, Y.-S.; McDaniel, H.; Robel, I.; Pietryga, J. M.; Klimov, V. I. Controlled Alloying of the Core−Shell Interface in CdSe/CdS Quantum Dots for Suppression of Auger Recombination. *ACS Nano* **2013**, *7*, 3411–3419.
35. Galland, C.; Ghosh, Y.; Steinbrück, A.; Sykora, M.; Hollingsworth, J. A.; Klimov, V. I.; Htoon, H. Two Types of

Luminescence Blinking Revealed by Spectroelectrochemistry of Single Quantum Dots. *Nature* **2011**, *479*, 203–207.
36. Rabouw, F. T.; Lunnemann, P.; van Dijk-Moes, R. J. A.; Frimmer, M.; Pietra, F.; Koenderink, A. F.; Vanmaekelbergh, D. Reduced Auger Recombination in Single CdSe/CdS Nanorods by One-Dimensional Electron Delocalization. *Nano Lett.* **2013**, *13*, 4884–489.
37. Klimov, V. I.; Ivanov, S. A.; Nanda, J.; Achermann, M.; Bezel, I.; McGuire, J. A.; Piryatinski, A. Single-Exciton Optical Gain in Semiconductor Nanocrystals. *Nature* **2007**, *447*, 441–446.
38. Achermann, M.; Hollingsworth, J. A.; Klimov, V. I. Multiexcitons Confined within a Subexcitonic Volume: Spectroscopic and Dynamical Signatures of Neutral and Charged Biexcitons in Ultrasmall Semiconductor Nanocrystals. *Phys. Rev. B* **2003**, *68*, 24530.
39. Caruge, J.-M.; Chan, Y.; Sundar, V.; Eisler, H. J.; Bawendi, M. G. Transient photoluminescence and simultaneous amplified spontaneous emission from multiexciton states in CdSe quantum dots. *Phys. Rev. B* **2004**, *70*, 08531.
40. Fisher, B.; Caruge, J. M.; Zehnder, D.; Bawendi, M. Room-Temperature Ordered Photon Emission from Multiexciton States in Single CdSe Core-Shell Nanocrystals. *Phys. Rev. Lett.* **2005**, *94*, 08740.
41. Bonati, C.; Mohamed, M. B.; Tonti, D.; Zgrablic, G.; Haacke, S.; van Mourik, F.; Chergui, M. Spectral and Dynamical Characterization of Multiexcitons in Colloidal CdSe Semiconductor Quantum Dots. *Phys. Rev. B* **2005**, *71*, 20531.
42. Zhao, J.; Nair, G.; Fisher, B. R.; Bawendi, M. G. Challenge to the Charging Model of Semiconductor-Nanocrystal Fluorescence Intermittency from Off-State Quantum Yields and Multiexciton Blinking. *Phys. Rev. Lett.* **2010**, *104*, 15740.
43. Norris, D. J.; Bawendi, M. G. Measurement and Assignment of the Size-Dependent Optical Spectrum in CdSe Quantum Dots. *Phys. Rev. B* **1996**, *53*, 16338–16346.
44. Van Embden, J.; Jasieniak, J.; Mulvaney, P. Mapping the Optical Properties of CdSe/CdS Heterostructure Nanocrystals: The Effects of Core Size and Shell Thickness. *J. Am. Chem. Soc.* **2009**, *131*, 14299–14309.
45. Efros, Al. L.; Rosen, M. The Electronic Structure of Semiconductor Nanocrystrals. *Annu. Rev. Mater. Sci.* **2000**, *30*, 475–521.
46. Franceschetti, A.; Troparevsky, M. C. Radiative Recombination of Triexcitons in CdSe Colloidal Quantum Dots. *J. Phys. Chem. C* **2007**, *111*, 6154–6157.
47. Beier, H. T.; Cote, G. L.; Meissner, K. E. Whispering Gallery Mode Biosensors Consisting of Quantum Dot-Embedded Microspheres. *Ann. Biomed. Eng.* **2009**, *37*, 1974–1983.
48. Gomez, D. E.; Pastoriza-Santos, I.; Mulvaney, P. Tunable Whispering Gallery Quantum-Dot-Doped Mode Emission from Microspheres. *Small* **2005**, *1*, 238–241.
49. Van Vugt, L. K.; Piccione, B.; Cho, C.-H.; Nukala, P.; Agarwal, R. One-Dimensional Polaritons with Size-Tunable and Enhanced Coupling Strengths in Semiconductor Nanowires. *Proc. Natl. Acad. Sci. U.S.A.* **2011**, *108*, 10050–10055.
50. Li, H. Y.; Rühle, S.; Khedoe, R.; Koenderink, A. F.; Vanmaekelbergh, D. Polarization, Microscopic Origin, and Mode Structure of Luminescence and Lasing from Single ZnO Nanowires. *Nano Lett.* **2009**, *9*, 3515–3520.
51. Peng, X. G.; Schlamp, M. C.; Kadavanich, A. V.; Alivisatos, A. P. Epitaxial Growth of Highly Luminescent CdSe/CdS Core/Shell Nanocrystals with Photostability and Electronic Accessibility. *J. Am. Chem. Soc.* **1997**, *119*, 7019–7029.
52. Nicolau, Y. F. Solution Deposition of Thin Solid Compound Films by a Successive Ionic-Layer Adsorption and Reaction Process. *Appl. Surf. Sci.* **1985**, *22−23*, 1061–1074.